Coulomb crystal mass spectrometry in a digital ion trap

Article (Published Version)

Coulomb crystal mass spectrometry in a digital ion trap

Nabanita Deb,[1] Laura L. Pollum,[1] Alexander D. Smith,[1] Matthias Keller,[2] Christopher J. Rennick,[1] Brianna R. Heazlewood,[1] and Timothy P. Softley[1,*]

[1]*Department of Chemistry, University of Oxford, Chemistry Research Laboratory, 12 Mansfield Road, Oxford OX1 3TA, United Kingdom*

[2]*Department of Physics and Astronomy, University of Sussex, Brighton BN1 9QH, United Kingdom*

(Received 25 September 2014; revised manuscript received 23 December 2014; published 24 March 2015)

We present a mass spectrometric technique for identifying the masses and relative abundances of Coulomb-crystallized ions held in a linear Paul trap. A digital radio-frequency wave form is employed to generate the trapping potential, as this can be cleanly switched off, and static dipolar fields are subsequently applied to the trap electrodes for ion ejection. Close to 100% detection efficiency is demonstrated for Ca^+ and CaF^+ ions from bicomponent Ca^+-CaF^+ Coulomb crystals prepared by the reaction of Ca^+ with CH_3F. A quantitative linear relationship is observed between ion number and the corresponding integrated time-of-flight (TOF) peak, independent of the ionic species. The technique is applicable to a diverse range of multicomponent Coulomb crystals—demonstrated here for Ca^+-NH_3^+-NH_4^+ and Ca^+-$CaOH^+$-$CaOD^+$ crystals—and will facilitate the measurement of ion-molecule reaction rates and branching ratios in complicated reaction systems.

DOI: 10.1103/PhysRevA.91.033408 PACS number(s): 37.10.Ty, 34.50.Lf, 82.30.Fi

I. INTRODUCTION

Recent improvements in cold molecular beam methods and their combination with ion traps are facilitating exciting new developments in the observation of cold, controlled ion-molecule reactions [1,2]. It is not sufficient, however, to simply conduct experiments in the cold regime; the resulting products must be quantitatively detected to extract information about the reaction process, such as the rate, the product branching ratio, and energy dependence.

Trapped, laser-cooled ions can undergo a phase transition to adopt a highly ordered "Coulomb crystal" structure. Cotrapped ions of a different species may be sympathetically cooled through elastic collisions with the laser-cooled ions, forming multicomponent Coulomb crystals. In this way, cold molecular ion targets of species that cannot be laser cooled can be prepared. Imaging the fluorescence continuously emitted by the laser-cooled ions enables real-time observation of the crystal framework, as depicted in Fig. 1(b). Due to the dependence of the trapping field on the charge-to-mass ratio of the ions, different ionic species are located in separate regions of the Coulomb crystal. In chemical reactions, this separation can be exploited and reaction rates can be measured through monitoring the changing shape of the crystal. For instance, the reaction of laser-cooled ions with neutral reactants—and the disappearance of fluorescing ions—is accompanied by changes in the crystal framework as product ions heavier (lighter) than the laser-cooled species migrate to the outer (inner) region of the crystal [1,3]. Hence, even though the nonfluorescing sympathetically cooled ions cannot be observed directly, comparison of molecular dynamics (MD) simulations with observed fluorescence images enables quantitative determination of ion numbers (see Fig. 1).

In complicated chemical systems with multiple product channels, however, MD simulations alone are insufficient for establishing accurate reaction rates. For example, in the reaction between $C_2H_2^+$ (sympathetically cooled into a Ca^+ Coulomb crystal) and NH_3, there are numerous exothermic pathways: proton transfer, charge transfer, two H-elimination pathways, and two H_2-elimination pathways [4]. In this case, both the reactant ions and numerous "dark" (nonfluorescing) product ions are lighter than the laser-cooled species, and thus would be indistinguishable in the dark inner core. A change in the ratio of the numbers of light ions of different mass would have little effect on the crystal framework. In some instances, resonant-excitation mass spectrometry (MS) methods can be utilized. The scanning of an additional radio-frequency (rf) field resonantly excites the secular motional frequencies of trapped ions, allowing the ion masses to be determined [5–7]. In the limiting case of a single molecular ion sympathetically cooled by a single laser-cooled ion, the mass of the molecular ion can be precisely measured, with for example $^{26}MgH^+$ and $^{26}MgD^+$ experimentally distinguishable [8]. While several variants of this nondestructive technique have been developed [9,10], resonant-excitation MS remains limited in application to small crystals with only a few different ion types; when motional frequency spectra are recorded for large multicomponent crystals, the features are poorly resolved and difficult to unambiguously assign, and the relative abundances cannot be ascertained quantitatively [3]. An alternative approach, termed ion crystal weighing, employs a pulsed electric field to excite the center-of-mass mode of the ions [11]. The frequency of the mode, and hence the mass of the crystal, can be deduced from the Fourier-transformed autocorrelation of the ion fluorescence signal. While ion crystal weighing is applicable to larger crystals, interpretation of the results is challenging when more than two ionic species are present or when the identities of the dark ions are unknown.

Adopting the principles of Wiley-McLaren time-of-flight MS (TOF-MS) [12], Hudson and co-workers recently demonstrated the ejection of ions from a linear Paul trap into a TOF tube and onto an external detector [13]. Ion ejection was achieved by switching off the rf voltages and converting the trap electrodes into a repeller-extractor pair by applying static voltages. However, when using resonantly driven cosine rf

*tim.softley@chem.ox.ac.uk

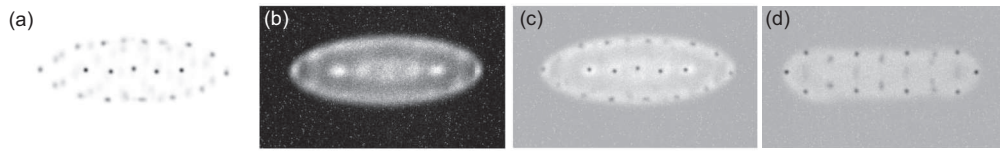

FIG. 1. The number of ions in a given Ca^+ Coulomb crystal can be established to within ± 5 ions by fitting the experimental image to MD simulations. A simulated crystal image with 50 Ca^+ ions is shown in panel (a), alongside an experimental Ca^+ crystal image in panel (b). The simulated crystal is overlaid on the experimental image in panel (c), illustrating the excellent agreement between the positions of the ions in the simulated and experimental crystals. This approach is also adopted for multicomponent crystals; in panel (d), a bicomponent Ca^+-CaF^+ experimental crystal (in which only the Ca^+ ions are fluorescing) is overlaid with a simulated Ca^+-CaF^+ crystal comprising 30 Ca^+ ions and 35 CaF^+ ions. Only the Ca^+ ions are made visible in the simulation, for ease of comparison between the images.

voltages, the trap electrodes form part of a resonant inductor-capacitor circuit. As the voltage is switched from cosine rf to direct current (dc), the amplitude of the trapping voltages decays with a time constant $1/k$ on the order of microseconds, and ringing of the form $V_{\rm rf}e^{-kt}\cos(\omega t)$ is superimposed on the ejection voltages. This compromises detection efficiency; ions experience vertical deflection away from the TOF axis and typically miss the detector. In an attempt to overcome this problem, Schneider and co-workers applied active damping and very high repeller and extractor voltages (1.4 and 1.2 kV, respectively). The observed mass-spectrum peak intensities, however, were not representative of the natural isotopic abundances of each species [13].

Quadrupole ion traps have been successfully combined with mass analysis apparatus in a variety of configurations—with ion ejection both along and perpendicular to the ion trap axis—and many such instruments are now commercially available [14,15]. Such systems, however, are not designed for the study of ion-molecule reactions in Coulomb crystals. There is insufficient optical access to the trap for effective laser cooling and crystal imaging. Furthermore, the typical operating pressures and repeated ejection cycles are not appropriate for the long storage times required in our experiments—we require ultrahigh vacuum (UHV) conditions to achieve ion storage times on the order of tens of minutes.

In this paper, we present a new digital ion trap (DIT) Wiley-McLaren MS technique for identifying the masses and relative abundances of all ions within a Coulomb crystal. Digital trapping wave forms, also termed square wave or pulsed wave forms, are applied to a linear Paul trap in place of the conventional cosine wave forms. This facilitates rapid, clean switching between the rf trapping and static dc ejection voltages, with no residual ringing. The entire crystal is ejected radially from the trap, where the ions pass through a TOF tube onto a microchannel plate (MCP) detector for mass-sensitive detection. The quantitative performance of the technique is characterized by the analysis of hundreds of Ca^+ and Ca^+-CaF^+ Coulomb crystals, in addition to multicomponent Ca^+-$CaOH^+$-$CaOD^+$ and Ca^+-$NH_3{}^+$-$NH_4{}^+$ crystals. The efficiency of ion ejection is studied, aided by extensive modeling. The methodology introduced in this work is applicable to any reaction of laser-cooled or sympathetically cooled ions, provided two conditions are satisfied: the cotrapped ions have an appropriate mass-to-charge ratio for efficient sympathetic cooling, and any product ions are formed with insufficient kinetic energy to escape the trap.

II. EXPERIMENTAL METHODS

The experiments presented in this paper utilize a linear Paul trap operated under UHV conditions, illustrated in Fig. 2. The cylindrical trap electrodes, 4 mm in radius, have a diagonal electrode-surface separation of $2r_0 = 7.0$ mm and are each composed of three segments (endcap separation $2z_0 = 5.5$ mm), to which a combination of rf and static voltages are applied. The conventional time-dependent trapping potential in a linear Paul trap is of the form $\phi_{\rm rf}(x,y,t) = \frac{V_{\rm rf}}{2}(\frac{x^2-y^2}{r_0^2})\cos(\omega_{\rm rf}t)$, with $V_{\rm rf}$ being the peak-to-peak voltage amplitude and $\omega_{\rm rf}$ the rf drive frequency. However, as first demonstrated in the 1970s [16,17], a cosine wave function is not essential for the generation of a trapping potential. A DIT, as we utilize in this work, employs a rectangular wave form of period T and a fractional pulse width τ, yielding a time-dependent trapping potential [18,19]:

$$\phi_{\rm rf}(x,y,t) = \frac{V_{\rm rf}}{2}\left(\frac{x^2-y^2}{r_0^2}\right)P_\tau(t), \tag{1}$$

$$P_\tau(t) = \begin{cases} 1 & \text{if } |t| \leqslant \tau T/2, \\ 0 & \text{if } \tau T/2 < |t| \leqslant (1-\tau)T/2, \\ -1 & \text{if } (1-\tau)T/2 < |t| \leqslant (1+\tau)T/2, \\ 0 & \text{if } (1+\tau)T/2 < |t| \leqslant (2-\tau)T/2, \\ 1 & \text{if } (2-\tau)T/2 < |t| \leqslant T, \end{cases} \tag{2}$$

$$P_\tau(t+T) = P_\tau(t), \tag{3}$$

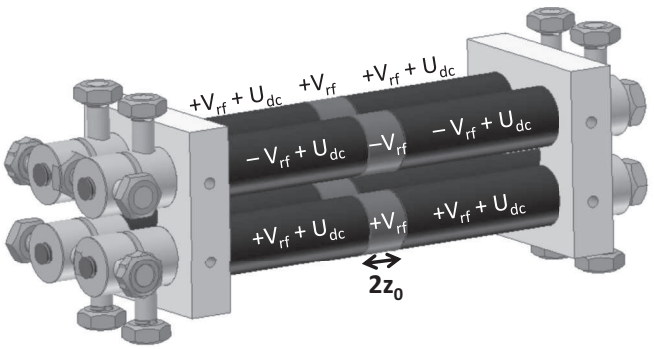

FIG. 2. Schematic illustration of the linear Paul trap utilized in this work, with four electrodes in a quadrupole arrangement. Each electrode is composed of three segments, with rf voltages ($V_{\rm rf}$) applied to all segments and additional dc voltages ($U_{\rm dc}$) applied to the endpieces.

where we can represent the pulsed wave form as the sum of its cosine Fourier components, $P_\tau(t) = \sum_{n=1}^{\infty} a_n \cos(n\omega_{\rm rf} t)$.

Axial confinement of ions in the trap is obtained through the application of static voltages ($U_{\rm dc}$) to the endpieces of the segmented electrodes, $\phi_{\rm end}(x,y,z) = \frac{\eta U_{\rm dc}}{z_0^2}(z^2 - \frac{x^2+y^2}{2})$, with $\eta = 0.244$ being a geometrical factor for this trap. The total electric potential is thus $\phi = \phi_{\rm rf}(x,y,t) + \phi_{\rm end}(x,y,z)$. The equations of motion for a single trapped ion can be expressed as a Hill differential equation (commonly known as a Mathieu equation for harmonic potentials), $d^2u/d\xi^2 + u[a_u + 2q_u f(\xi)] = 0$, where $f(\xi) = \cos(2\xi)$ for a cosine rf field and $f(\xi) = P_\tau(\xi)$ for a digital rf field, $u \in [x,y]$, and $\xi = \frac{1}{2}\omega_{\rm rf} t$. The stability of an ion trajectory is dependent on the dimensionless trapping parameters a_u and q_u. The (q_u, a_u) plane is divided into stable and unstable regions; for stable values of a_u and q_u, the solutions to the equations of motion are bound and the ion will be confined in the trap. In a DIT, the Hill differential equations are dependent on the fractional pulse width (τ), which can be varied to yield a stability diagram comparable to that of a cosine trap. (See Ref. [18] for a derivation of the stability criterion in a DIT.) Bandelow *et al.* have recently experimentally confirmed the applicability of the a_u and q_u parameters in mapping the stability regions of a hyperbolic Paul DIT [20,21].

We can define dimensionless stability parameters that are dependent on the mass (m) and charge (Q) of the species [2,18],

$$a_x = a_y = -\frac{\eta 4 Q U_{\rm dc}}{m z_0^2 \omega_{\rm rf}^2}, \tag{4}$$

$$q_x = -q_y = -\frac{2 Q V_{\rm rf}}{m r_0^2 \omega_{\rm rf}^2}, \tag{5}$$

which enable one to construct a DIT stability diagram in terms of $U_{\rm dc}$ and $V_{\rm rf}$ (see Fig. 3). From the secular potential, defined as the sum of the pseudopotential (the harmonic time-averaged potential arising from the oscillating rf fields) and the static endpiece potential, one can derive the digital trap depth,

$$\phi_{\rm sec}(r_0) = c\frac{Q^2}{2m\omega_{\rm rf}^2}\frac{V_{\rm rf}^2}{r_0^2} - \frac{\eta Q U_{\rm dc} r_0^2}{2 z_0^2}, \tag{6}$$

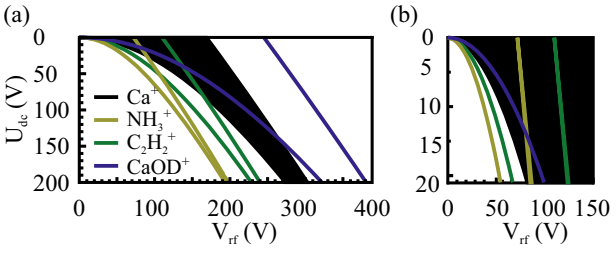

FIG. 3. (Color online) (a) The regions of stability for several ionic species in the DIT operating at $\tau = 0.25$ and $\omega_{\rm rf} = 2\pi \times 1.33$ MHz. For clarity, only the stability region of Ca^+ is shaded black; for all other species, the stability region is enclosed between the relevant colored (shaded) curves. Regions of overlapping stability indicate the operating parameters ($V_{\rm rf}, U_{\rm dc}$) where species can be cotrapped. (b) A closer view of the experimentally accessible region of the stability diagram.

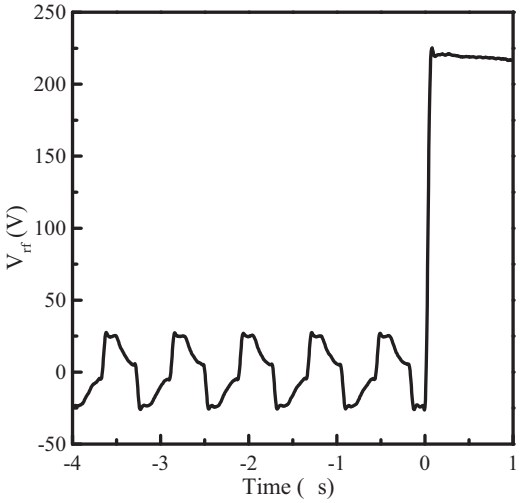

FIG. 4. Experimental digital rf trapping wave form (−4 to 0 μs) and ejection pulse (0 μs onwards).

with $c = \frac{1}{2}\sum_{n=1}^{\infty} a_n^2/n^2$ being a sum over the Fourier-component amplitudes a_n. In a DIT, $a_n = \frac{4}{n\pi}\sin(n\pi\tau)$ (where $n \in$ odd) and thus the trap depth depends on the fractional pulse width τ; in a cosine trap, $c = 0.5$. The digital rf voltage is applied at a frequency of $\omega_{\rm rf} = 2\pi \times 1.33$ MHz, with typical trap parameters $V_{\rm rf} = 50$ V, $U_{\rm dc} = 1.0$ V, and $\tau = 0.25$ yielding a_u and q_u values that fall within the regions of stability for all ionic species considered in this work.

The experimental digital wave form (Fig. 4) exhibits a nonzero pulse decay time and thus deviates from the ideal digital wave form. MD simulations—in which the measured digital wave form can be directly utilized—indicate that this deviation from the ideal wave form has a very minor impact on the trap depth and does not adversely affect crystal formation, crystal stability, or the ejection properties of the system. This is in agreement with Sudakov and Nikolaev, who found nonideal wave forms to have an insignificant effect on the calculated regions of stability in a DIT [22]. Hence assuming the real digital wave form is well represented by an ideal digital wave form, a trap depth of ∼1.21 eV is calculated—shallower than the cosine trap depth of ∼1.36 eV as previously utilized in our research group [23], but entirely sufficient for most applications.

To form Coulomb crystals, calcium atoms in an effusive skimmed beam are nonresonantly ionized (at 355 nm) in the trap center. The resulting Ca^+ ions are laser cooled on the $4s\,^2S_{1/2} \rightarrow 4p\,^2P_{1/2}$ transition at 397 nm, with a 866-nm repump beam addressing population lost to the $3d\,^2D_{3/2}$ state. The cooling lasers are reflected back along the trap axis to achieve bidirectional cooling. An additional 397-nm beam at 45° to the trap axis provides radial cooling. Fluorescence continuously emitted by laser-cooled Ca^+ ions is imaged by a lens into an intensified charge-coupled device camera system, yielding a two-dimensional image of the Coulomb crystal. High-precision leak valves facilitate the controlled introduction of neutral reactants into the ion trap chamber, typically held at pressures of $\sim 1 \times 10^{-9}$ mbar. In this way, we generate molecular ions through chemical reactions between

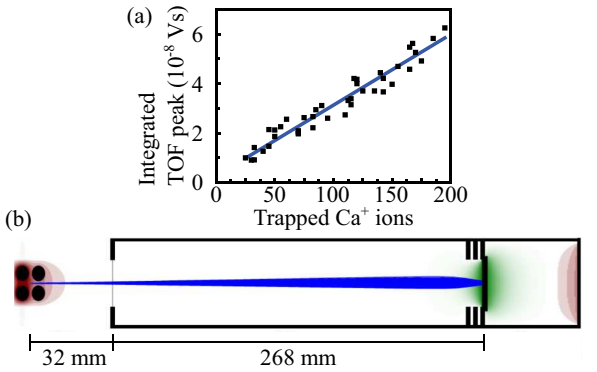

FIG. 5. (Color online) (a) The integrated Ca^+ peak intensity in the TOF spectrum is plotted for each Coulomb crystal against the number of Ca^+ ions, determined from fitting the experimental images to MD simulations. (b) Schematic illustration of the TOF-MS apparatus, depicting the ion trap electrodes (viewed along the trap axis, with ion ejection perpendicular to this axis), TOF tube, and MCPs. Trajectories of 200 Ca^+ ions ejected from the trap are shown (in blue online) from the ion trap (left) to the front detector plate (right). The electric potential near the ion trap is positive (shaded red online) and near the front detector plate is negative (shaded green online).

the neutral reactant gas and trapped Ca^+ ions, or with trapped sympathetically cooled ions.

After the quadrupole trapping voltages are switched off, ions are radially ejected into the TOF tube by dipolar repeller and extractor fields of +220 and +97 V, respectively, applied with a rise time of 70 ns, and are accelerated towards a grounded mesh of 88% transparency mounted across the entrance of the TOF tube [see Fig. 5(b)]. The ions are detected by a MCP detector at the end of the flight tube. The repeller and extractor voltages employed were found empirically to give the best TOF mass resolution for Ca^+, and this two-stage acceleration arrangement is equivalent to a Wiley-McLaren TOF scheme [12]. In the experiments reported here there was (nominally) zero delay in the switching from the trapping voltages to the ejection voltages (see Fig. 4); although the delay can be varied easily in the digital trap, minimizing the delay was found to optimize the mass resolution.

III. SIMULATIONS

Coulomb crystals are simulated using a custom-written MD crystal simulation program, which takes the experimental digital wave form as the input rf trapping voltage. Simulated crystal images can thus be directly compared to those observed experimentally, as demonstrated in Fig. 1. A MATLAB program is used to model the ion trajectories upon ejection by calculating the electric fields in the ion trap and the TOF tube, using SIMION to solve the Laplace equation numerically and including ion-ion repulsion. Taking the identity, position, and velocity of each ion within a Coulomb crystal (as output by the MD code) and the experimental ejection voltages as input parameters, ion trajectories are calculated using a velocity Verlet algorithm [24,25]. For Coulomb crystals composed of $\leqslant$200 ions, simulations indicate that the detection efficiency is limited only by the transmittance of the grounded mesh; detection efficiency is independent of the particular species, for all species considered in this work.

IV. RESULTS AND DISCUSSION

To verify the predicted detection efficiency experimentally, the number of Ca^+ ions in a given crystal is determined for several hundred Coulomb crystals of various sizes by comparing the experimental image immediately prior to ejection to a set of simulated crystal images (see Fig. 1). Following crystal ejection, the area under the relevant mass peak is calculated by integration of the (background-subtracted) TOF trace. Figure 5(a) illustrates the linear correlation between the number of ions in a Ca^+ Coulomb crystal and the integrated TOF peak recorded upon crystal ejection, for up to 200-ion crystals. The measurement error is governed by the uncertainty in the comparison between an experimental crystal and its MD simulation (±5 ions). The mass resolving power of the technique, defined as $m/\Delta m$ where Δm is the full width at half maximum of the mass spectrum peak, is 90 for a typical 100-ion Ca^+ crystal and >70 for all Ca^+ crystals containing up to 200 ions: The slightly lower resolving power for larger crystals is due to the greater spread of initial positions and velocities in those cases. Crystals with more than 200 ions were not considered experimentally due to imaging limitations; the objective lens and camera restrict the field of view.

To establish the applicability of this DIT MS technique to multicomponent Coulomb crystals, mixed crystals of Ca^+ and CaF^+ are prepared by admitting a low pressure of CH_3F gas to the ion trap chamber, leading to the reaction $Ca^+ +$

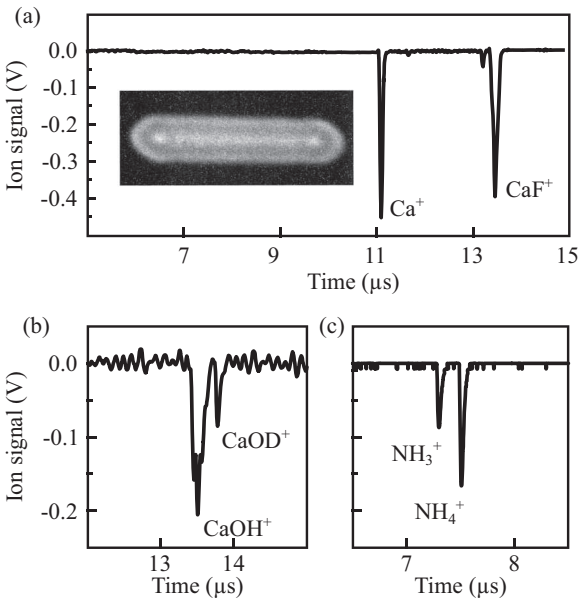

FIG. 6. (a) A bicomponent Ca^+-CaF^+ Coulomb crystal and the TOF trace recorded following ejection of the crystal. Peaks arising from species with masses differing by 1 u can be resolved, as demonstrated by the ejection of (b) Ca^+-$CaOH^+$-$CaOD^+$ and (c) Ca^+-NH_3^+-NH_4^+ multicomponent crystals. The two unlabeled small peaks in panel (a) are due to unidentified minor impurities.

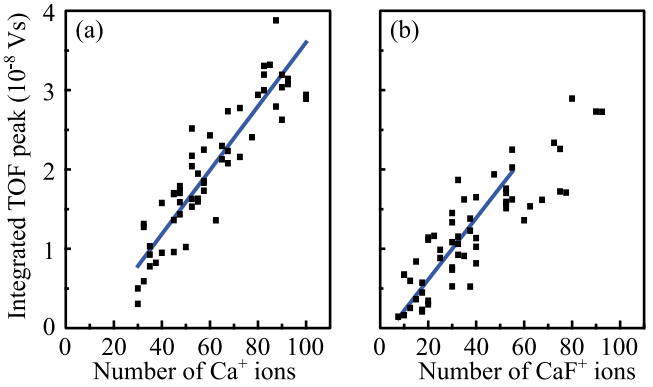

FIG. 7. (Color online) Bicomponent Ca^+-CaF^+ crystal ejection analysis. The integrated TOF peak for (a) Ca^+ and (b) CaF^+ ions is plotted against the number of ions of that species in each crystal, ascertained from fitting the crystal images to simulations, for bicomponent crystals of various sizes and compositions.

$CH_3F \rightarrow CaF^+ + CH_3$. The resulting CaF^+ product ions sympathetically cool into the Ca^+ Coulomb crystal, forming a dark outer shell—indicated by the flattening of the fluorescing Ca^+ core in the crystal images [see Figs. 1(d) and 6(a)]. Repeating simulations for variable numbers of laser-cooled ions and dark ions enables a determination of the number of each species in the crystal, assuming there is only one "dark" component. The mass-to-charge ratio of CaF^+:Ca^+ is 1.475, well within the desired range for optimal sympathetic cooling [1,2], and this work demonstrates that multicomponent Coulomb crystals can be formed in a DIT.

As Fig. 7 illustrates, a linear relationship is observed between the integrated TOF mass peaks and ion numbers—for both the fluorescing Ca^+ and the nonfluorescing CaF^+ ions. The gradients of the lines-of-best-fit, $(4.0 \pm 0.2) \times 10^{-10}$ Vs ion^{-1} for Ca^+ and $(3.9 \pm 0.4) \times 10^{-10}$ Vs ion^{-1} for CaF^+ (for up to 60 CaF^+ ions), established using a linear least-squares fitting procedure with uncertainties considered in both coordinates, are in quantitative agreement. These results are also in quantitative agreement with the Ca^+-only crystal results shown in Fig. 5(a), demonstrating the utility of the technique: equal detection efficiency is observed regardless of ion mass. There are too few crystals in the data set with $\geqslant$60 CaF^+ ions to extend the trend further, and the precision with which CaF^+ ion numbers can be estimated from simulations decreases at higher CaF^+:Ca^+ ratios. Trajectory simulations indicate that the observed linear trend will hold for larger numbers of ions (up to 400-ion crystals), and for a diverse range of ionic species, provided the mass-to-charge ratios of cotrapped species are similar and there are a sufficient number of laser-cooled ions for efficient sympathetic cooling.

The mass resolution is investigated by the ejection of crystals containing species differing in mass by 1 u. Tricomponent Ca^+-$CaOH^+$-$CaOD^+$ crystals are formed in a two-step process. H_2O vapor is admitted to the chamber through a leak valve, where reaction with Ca^+ (in the $3d\,^2D$ excited states populated by the laser-cooling process) [26] yields $CaOH^+$ molecular ions. D_2O is then admitted through a second leak valve, forming $CaOD^+$ ions. As Fig. 6(b) illustrates, peaks arising from $CaOH^+$ and $CaOD^+$ are resolved in the spectrum, indicating a resolution better than 1 mass unit at 58 u.

The applicability of this DIT MS technique for species lighter than Ca^+ is confirmed with tricomponent Ca^+-$NH_3{}^+$-$NH_4{}^+$ Coulomb crystals. NH_3 is resonantly ionized at 312.5 nm, with some of the sympathetically cooled NH_3^+ ions subsequently reacting with neutral NH_3 to form NH_4^+, yielding tricomponent crystals. Following the same imaging and ejection process detailed above, the TOF spectra again exhibit well-resolved peaks, as shown in Fig. 6(c). In this system, both the dark species are lighter than Ca^+. Accordingly, conventional comparisons of the experimental crystals with simulated images do not reveal the relative numbers of $NH_3{}^+$ and $NH_4{}^+$ ions, as both species are located in the dark inner core. The same applies to multicomponent Ca^+-$CaOH^+$-$CaOD^+$ crystals, where the $CaOH^+$ and $CaOD^+$ species are both heavier than Ca^+ and therefore are both located in the dark outer shell. DIT MS enables us to acertain the relative numbers of dark ions which are otherwise indistinguishable in the experimental and simulated images.

V. CONCLUSIONS

In summary, we have established DIT MS to be a robust technique for the quantitative characterization of multicomponent Coulomb crystals produced, in this work, by chemical reactions of the trapped ions. The ejection process is efficient, with a linear correlation between the number of ions ejected and the corresponding integrated TOF peak, and a detection efficiency that is independent of the crystal size or the ionic species involved. The DIT MS technique is applicable to a diverse range of multicomponent Coulomb crystals and hence to a diverse range of chemical reactions—not only reactions of laser-cooled ions but also of sympathetically cooled ions. While the ejection process is destructive, repeating the process with reloaded crystals at a range of reaction times allows the determination of accurate reaction rates and branching ratios in complicated ion-molecule reactions. With the ability to unambiguously detect both the masses and the relative numbers of trapped ions, DIT MS has the potential to be a powerful detection technique in the study of sympathetically cooled molecular ion reactions—utilized as a stand-alone method or in combination with existing techniques such as MD simulations.

ACKNOWLEDGMENTS

T.P.S. acknowledges the financial support of the EPSRC under Grants No. EP/G00224X/1 and No. EP/I029109. N.D. is grateful for support from the Felix Scholarships Foundation, L.L.P. for support from the Clarendon Fund, C.J.R. for support from the Ramsay Memorial Trust, and B.R.H. for support from the Royal Commission for the Exhibition of 1851 and the EU Marie Curie Career Integration Grant Scheme (Grant No. PCIG13-GA-2013-618156).

[1] B. R. Heazlewood and T. P. Softley, Low-temperature kinetics and dynamics with Coulomb crystals, Annu. Rev. Phys. Chem. **66** (2015), doi:10.1146/annurev-physchem-040214-121527

[2] S. Willitsch, Coulomb-crystallised molecular ions in traps: Methods, applications, prospects, Int. Rev. Phys. Chem. **31**, 175 (2012).

[3] S. Willitsch, M. T. Bell, A. D. Gingell, and T. P. Softley, Chemical applications of laser- and sympathetically-cooled ions in ion traps, Phys. Chem. Chem. Phys. **10**, 7200 (2008).

[4] J. Qian, H. Fu, and S. L. Anderson, Dynamics of the $C_2H_2^+ + ND_3$ reaction: A vibrational-mode-selective scattering study, J. Phys. Chem. A **101**, 6504 (1997).

[5] T. Baba and I. Waki, Cooling and mass-analysis of molecules using laser-cooled atoms, Jpn. J. Appl. Phys. **35**, L1134 (1996).

[6] M. Welling, H. A. Schuessler, R. I. Thompson, and H. Walther, Ion/molecule reactions, mass spectrometry and optical spectroscopy in a linear ion trap, Int. J. Mass Spectrom. Ion Process. **172**, 95 (1998).

[7] M. Drewsen, A. Mortensen, R. Martinussen, P. Staanum, and J. L. Sorensen, Nondestructive identification of cold and extremely localized single molecular ions, Phys. Rev. Lett. **93**, 243201 (2004).

[8] P.F. Staanum, K. Hojbjerre, R. Wester, and M. Drewsen, Probing isotope effects in chemical reactions using single ions, Phys. Rev. Lett. **100**, 243003 (2008).

[9] B. Roth, A. Ostendorf, H. Wenz, and S. Schiller, Production of large molecular ion crystals via sympathetically cooling by laser-cooled Ba^+, J. Phys. B **38**, 3673 (2005).

[10] C. Raab, J. Eschner, J. Bolle, H. Oberst, F. Schmidt-Kaler, and R. Blatt, Motional sidebands and direct measurement of the cooling rate in the resonant fluorescence of a single trapped ion, Phys. Rev. Lett. **85**, 538 (2000).

[11] K. Sheridan and M. Keller, Weighing of trapped ion crystals and its applications, New J. Phys. **13**, 123002 (2011).

[12] W. C. Wiley and I. H. McLaren, Time-of-flight mass spectrometer with improved resolution, Rev. Sci. Instrum. **26**, 1150 (1955).

[13] C. Schneider, S. J. Schowalter, K. Chen, S. T. Sullivan, and E. R. Hudson, Laser-cooling-assisted mass spectrometry, Phys. Rev. Appl. **2**, 034013 (2014).

[14] S. M. Michael, M. Chien, and D. M. Lubman, An ion trap storage/time-of-flight mass spectrometer, Rev. Sci. Instrum. **63**, 4277 (1992).

[15] Q. Hu, R. J. Noll, H. Li, A. Makarov, M. Hardman, and R. G. Cooks, The Orbitrap: A new mass spectrometer, J. Mass Spectrom. **40**, 430 (2005).

[16] J. A. Richards, R. M. Huey, and J. Hiller, A new operating mode for the quadrupole mass filter, Int. J. Mass Spectrom. Ion Phys. **12**, 317 (1973).

[17] E. P. Sheretov, Some properties of charged particle trajectories in quadrupole mass spectrometers: Part I. General theory, Int. J. Mass Spectrom. **219**, 315 (2002).

[18] N. Kjaergaard and M. Drewsen, Crystalline beam emulations in a pulse-excited linear Paul trap, Phys. Plasmas **8**, 1371 (2001).

[19] N. Kjaergaard and M. Drewsen, Observation of a structural transition for Coulomb crystals in a linear Paul trap, Phys. Rev. Lett. **91**, 095002 (2003).

[20] S. Bandelow, G. Marx, and L. Schweikhard, The stability diagram of the digital ion trap, Int. J. Mass Spectrom. **336**, 47 (2013).

[21] S. Bandelow, G. Marx, and L. Schweikhard, The 3-state digital ion trap, Int. J. Mass Spectrom. **353**, 49 (2013).

[22] M. Sudakov and E. Nikolaev, Ion motion stability diagram for distorted square waveform trapping voltage, Eur. J. Mass Spectrom. **8**, 191 (2002).

[23] S. Willitsch, M. T. Bell, A. D. Gingell, S. R. Procter, and T. P. Softley, Cold reactive collisions between laser-cooled ions and velocity-selected neutral molecules, Phys. Rev. Lett. **100**, 043203 (2008).

[24] L. Verlet, Computer "experiments" on classical fluids. I. Thermodynamical properties of Lennard-Jones molecules, Phys. Rev. **159**, 98 (1967).

[25] W. C. Swope, H. C. Anderson, P. H. Berens, and K. R. Wilson, A computer simulation method for the calculation of equilibrium constants for the formation of physical clusters of molecules: Application to small water clusters, J. Chem. Phys. **76**, 637 (1982).

[26] K. Okada, M. Wada, L. Boesten, T. Nakamura, I. Katayama, and S. Ohtani, Acceleration of the chemical reaction of trapped Ca^+ ions with H_2O molecules by laser excitation, J. Phys. B **36**, 33 (2003).